SKI Technical Report 91:17

The Motion of a Redox Front in a System of Bentonite and Rock, Incorporating Fracture Transport Effects

W. Shaw
P. Robinson

February 1992

SKi
STATENS KÄRNKRAFTINSPEKTION
SWEDISH NUCLEAR POWER INSPECTORATE

The Motion of a Redox Front in a System of Bentonite and Rock, Incorporationg Fracture Transport Effects

W. Shaw - P. Robinson

SKI TR 91:17

Intera Environmental Division
Chiltern House
45 Station Road
Henley-on-Thames
Oxfordshire
RG9 1AT

February 1992

Redox Front Motion with Fracture Transport Effects

Summary

This report presents new calculations of the motion of a redox front in a system of bentonite and fractured rock, incorporating advection and diffusion of oxidants in fracture water. The results reported here have been incorporated into preliminary base case calculations using the source term model CALIBRE.

The model presented here differs mainly in its treatment of the effects of the fracture. Previously, a "zero-concentration" boundary condition was applied, and this resulted in retardation of the front near the fracture. When a more detailed advection-diffusion model is applied, the front is advanced in a neighbourhood of the fracture.

Contents

List of Figures

List of Tables

1 Introduction

This document constitutes the first of two final reports on the modelling of the oxidation state of the near-field environment within the CALIBRE Source Term Model. The specifiifcation of CALIBRE was orginally set out in [1], and has been developed within the context of studies into the Swedish spent fuel disposal concept [2]. It has been prepared by Intera Environmental Division under contract to the Swedish Nuclear Power Inspectorate (SKI). Preliminary results about the near-field oxidation state were presented in [3]. This document should also be read in conjunction with the second final report on the redox front [4].

The first part of the CALIBRE program concerns the diffusion of oxidants into a reducing environment, and is formulated as a series of diffusion problems with a chemical reaction at a moving front. The knowledge of the progress of the front forms a necessary ingredient for CALIBRE, since the solubility limits of significant radionuclides are sensitive to the redox potential of the medium through which they are being transported.

During the course of the development of CALIBRE, a recurrent issue has been the boundary conditions to be applied at the fracture. This has affected both the redox and radionuclide transport components of CALIBRE. In each case, the original scheme assumed that fast flow rates in the fracture would allow the simplification of introducing zero-concentration boundary conditions, for both oxidants and radionclides. During the course of preliminary calculations on both parts of the model, this assumption has been questioned and the consequences of dropping it considered. The evolution of the radionuclide transport component of the code in this way is chronicled in [5].

For the oxidation state, some initial calculations were carried out with a zero concentration boundary condition, and these, together with the basic technical description of the redox model, are described in [3]. This final technical description of the model, includes some results from calculations (the preliminary base cases) where the boundary condition involved coupling to transport in the fracture.

In the preliminary specification of the model [1] the equations of motion for the front were given. In Section two this specification is presented in revised form for the front motion problem with fracture effects included. The problem is summarized graphically by Figure 1. Originally, a zero concentration boundary condition was applied. In the analysis presented here, the capacity of the fracture for transporting oxidants is taken into account in a more general framework. The fracture oxidant transport is

described by an advection-diffusion equation. Since the underlying model treats only the radial and vertical geometry, the advection term cannot be fully represented without approximation, since it destroys the radial symmetry.

Of course, this issue must be faced in the treatment of the radionuclide transport, as well as the redox front computation. To handle this, a modification of the radial equations, which includes an approximation to advective transport in the fracture, has been introduced and is described in [5]. The same approach is employed here. The basic computational approach adopted (the application of the "enthalpy" approach) could be generalized to a full three-dimensional model, but this would require a major increase in computation time, and in order to be most efficient, a re-appraisal of the details of the numerical scheme. The other significant limitation of the approach described in this document is that the presence of reducing agents in the fracture water has not been modelled. This effect is discussed in the second final report, but only on the basis of simple scoping calculations. This could be accounted for in a full 3D model, but again, only at the expense of further calculational complexity.

Section three describes a suite of analytical and numerical devices which collectively allow the solution to the problem to be extracted. An initial approach considered in [1], based on the "quasi-stationary" approximation technique, applied before in the redox context in [6] , was found to be insufficiently general in the present problem. The difficulty is that the parameters of the problem, reproduced here in summary form in Table 4, were found to be such that the problem *may* be outside the domain of applicabilty of quasi-stationary methods. This possibility was noted in [1], and a full description of the parameters of the entire model is given in [7]. Even when the parameter ranges fall within the domain of applicability of quasi-stationary methods, such approximations may fail to capture all of the dynamical properties of the front and the associated oxidant concentration profile.

The solution procedure adopted may be summarized as follows. In the bentonite, successive improvements to the quasi-stationary method leads to an exact formulation of the problem in terms of integral equations, valid for all parameter values. It is possible to extract, from these equations, estimates for the front location under a variety of circumstances. For the full 2-dimensional problem where the front is in the rock-fracture system, a numerical scheme has been devised. The scheme is based on an "enthalpy" method, and requires no restrictions on parameter values, or approximations other than those involved in discretizing the problem. This scheme has been coded, and the resulting program verified by comparison with the analytical estimates obtained for the initial radial motion

of the front within the bentonite. The program is capable of calculating the front profile as a function of time, and, since the oxidant concentration is also available, quantities of interest such as the oxidant flux in the fracture.

The development of these tools has drawn on several sources. The analytical devices are based on ideas developed in [8] - [14]. The numerical scheme has its roots in the ideas of [15] and [16], and the particular scheme employed here is one of those described in [17]. The discussions of radial diffusion in bentonite make considerable use of properties of Bessel functions, as described, e.g. in [18]. Also, gratitude is expressed for advice, regarding these techniques, from Dr. J.R. Ockendon and Dr. J.N. Dewynne at the Mathematical Institute, Oxford, and Prof. I. Neretnieks, of the Royal Institute of Technology, Sweden.

The verification of the numerical scheme against the analytical methods is described in Section four. The application of the method to the problem of immediate interest is outlined in Section five, where a qualitative description of the behaviour of the front motion is given. Results for the preliminary base case calculations are also presented in Section five. These results were used as an input to the preliminary radionuclide transport calculations presented in [19].

In the second final report on the oxidation issues, the results here are complemented by a discussion of the final base case calculations, including a new oxidant production rate based on new inventory data; the final results; a discussion of the state of the fracture based on chemistry scoping calculations; and, a simple model of a front crossing an interface, such as that between bentonite and rock.

2 Background

2.1 The Model and Initial Processes

The approach taken here is to set up a reasonably complete mathematical model of the front motion, following [1], which consequently establishes which parameters are of interest for understanding the front motion. A discussion of the values and uncertainties associated with the various parameters will be given in section 2.5. The initial values of the estimates and associated uncertainties, used in the original analysis of the problem given in [3], are sumarized in Table 4.

The starting point for this stage of the modelling is the breach of the canister containing the waste. Once the canister has been breached, it is assumed that water is in intimate contact with the fuel. Radiation breaks down some of the water molecules to produce oxidants, notably hydrogen peroxide.

The net production rate of oxidants per unit volume, $G_{ox}(t)$ kmol.m^{-3}.s^{-1} is determined primarily by the alpha radiation field in the vicinity of fuel particles, the thickness of the water film on those particles and the water chemistry, such as the Fe^{2+} concentration. These processes have been investigated by Christensen et al [20, 21, 22].

On a slightly longer timescale, oxidants may be consumed by reducing agents such as metals in the solid waste, matrix and canister material. These materials are assumed to have a finite capacity for the reduction of oxidants. Moreover this reaction is assumed to take place rapidly in comparison to the timescales of interest for radionuclide release, but at a slower rate than reactions with reducing agents such as Fe^{2+} in the water. Consequently, conditions within the canister will not become fully oxidising until a time T_2 when all the available reducing agents in the solids inside the canister have been used up. This time is therefore defined by the equation

$$\int_{T_i}^{T_2} G_{ox}(t)\,dt = Q^C. \tag{2.1}$$

where Q^C is the amount of oxidant which can be reduced per unit volume of the canister.

2.2 Canister Effects

Beyond the time T_2, oxidants are assumed to build up in the water-filled pore space of the degraded canister and be dissipated by radial diffusion through the bentonite. The average oxidant concentration in the canister pore water (C^C_{ox}) is then determined by

$$\varepsilon^C \frac{dC^C_{ox}(t)}{dt} = G_{ox}(t) - \frac{A}{V} F_{ox}(t), \tag{2.2}$$

for $t > T_2$ where ε^C is the porosity of the degraded canister and V and A are its volume ($\pi r_1^2 L$) and cylindrical surface area ($2\pi r_1 L$) respectively. The radial diffusive flux of oxidant, $F_{ox}(t)$, is defined in the next section.

These oxidising species diffuse through the pore water of the bentonite. During this process they are assumed to react instantaneously with reducing agents, such as ferrous iron, in the bentonite. Thus a sharp redox front is formed separating the oxidising and reducing species. This front moves slowly through the bentonite as more oxidising species are generated. It then passes into the rock-fracture system, where the behaviour of the system becomes essentially 2-dimensional. The rock-fracture system is such that many fractures intersect the neighbourhood of the canister and associated bentonite. As discussed in Section 1, this system will be idealized by regarding the fractures as being bounded by horizontal planes with normals along the canister axis. These planes are treated as being periodically spaced in the canister axis direction, with the fracture thickness much less than the inter-fracture spacing. The full problem may then be replaced by an equivalent micro-problem on a domain limited to half an inter-fracture region. The essential features of this micro-problem are summarized by Figure 1.

2.3 Redox Front in the Bentonite

In the initial phase the redox front moves radially through the bentonite. The basic equation describing the oxidant concentration in the bentonite pore water ($C^B_{ox}(r,t)$) is

$$\varepsilon^B \frac{\partial C^B_{ox}(r,t)}{\partial t} = \frac{D^B_{ox}}{r} \frac{\partial}{\partial r} \left(r \frac{\partial C^B_{ox}(r,t)}{\partial r} \right). \tag{2.3}$$

for times and positions such that $t > T_2$ and

$$r_1 < r < r^B_{ox}(t) < r_2, \tag{2.4}$$

where ε^B is the porosity and D^B_{ox} is the intrinsic diffusivity of the bentonite.

At the redox front ($r_{ox}^{B}(t)$) the oxidant concentration is zero.

$$C_{ox}^{B}(r_{ox}^{B}(t), t) = 0. \tag{2.5}$$

The movement of the redox front is determined by a balance between the rate at which oxidants diffuse to the front and the reducing capacity of the bentonite:

$$\frac{dr_{ox}^{B}(t)}{dt} = -\frac{D_{ox}^{B}}{Q^{B}} \frac{\partial C_{ox}^{B}(r, t)}{\partial r}\bigg|_{r=r_{ox}^{B}(t)}. \tag{2.6}$$

where Q^{B} is the amount of oxidant which can be reduced per unit volume of bentonite. At the boundary between the bentonite and the canister we have

$$D_{ox}^{B} \frac{\partial C_{ox}^{B}(r, t)}{\partial r}\bigg|_{r=r_1} = -F_{ox}(t). \tag{2.7}$$

and

$$C_{ox}^{C}(t) = C_{ox}^{B}(r_1, t). \tag{2.8}$$

The initial conditions are

$$C_{ox}^{B}(r, t=T_2) = 0. \tag{2.9}$$

and

$$r_{ox}^{B}(t=T_2) = r_1. \tag{2.10}$$

2.4 Redox Front in the Rock-Fracture System

When the redox front reaches the edge of the deposition hole the transport of oxidants ceases to be radially symmetric. This occurs at a time $t=T_3$ when $r_{ox}^{B}(t = T_3) = r_2$. In the present approximation scheme the axial (z) dependence now comes into play. The following system of equations governs the evolution of the oxidant concentration in the bentonite and the rock associated with it. The geometry of the system is as shown in Figure 1.

In the bentonite

$$\varepsilon^{B} \frac{\partial C_{ox}^{B}(r, z, t)}{\partial t} = D_{ox}^{B} \left[\frac{1}{r} \frac{\partial}{\partial r} \left(r \frac{\partial C_{ox}^{B}(r, z, t)}{\partial r} \right) + \frac{\partial^2 C_{ox}^{B}(r, z, t)}{\partial z^2} \right], \tag{2.11}$$

for

$$\left.\begin{aligned} r_1 < r < r_2. \\ 0 < z < Z. \end{aligned}\right\} \tag{2.12}$$

where Z is one half of the inter-fracture spacing. The canister wall boundary conditions, (2.7) and (2.8), still apply. At the mid-plane between two fractures ($z=Z$) and in the mid-plane of the fracture ($z=0$) symmetry boundary conditions are applied, namely

$$\left.\frac{\partial C_{ox}^{B}(r,z,t)}{\partial z}\right|_{z=0} = \left.\frac{\partial C_{ox}^{B}(r,z,t)}{\partial z}\right|_{z=Z} = 0. \tag{2.13}$$

In the rock matrix the oxidant pore water concentration (C_{ox}^{R}) is determined by

$$\varepsilon^{R}\frac{\partial C_{ox}^{R}(r,z,t)}{\partial t} = D_{ox}^{R}\left[\frac{1}{r}\frac{\partial}{\partial r}\left(r\frac{\partial C_{ox}^{R}(r,z,t)}{\partial r}\right) + \frac{\partial^2 C_{ox}^{R}(r,z,t)}{\partial z^2}\right], \tag{2.14}$$

for

$$\left.\begin{aligned} r_2 < r < r_{ox}^{R}(z,t), \\ b < z < Z, \end{aligned}\right\} \tag{2.15}$$

where b is the fracture half-width.

At the redox front ($r_{ox}^{R}(z,t)$) the oxidant concentration is zero,

$$C_{ox}^{R}(r_{ox}^{R}(z,t),z,t) = 0. \tag{2.16}$$

Its position is determined by

$$v_n = -\frac{D_{ox}^{R}}{Q^{R}}\left.\frac{\partial C_{ox}^{R}(r,z,t)}{\partial n}\right|_{r=r_{ox}^{R}(z,t)}, \tag{2.17}$$

where $\frac{\partial}{\partial n}$ indicates the derivative normal to the redox surface, D_{ox}^{R}, C_{ox}^{R} are analogous to D_{ox}^{B}, C_{ox}^{B}, and v_n denotes the speed of the front in the direction normal to the front. (Note that equation constitutes an amendment to the corresponding equation (4.17) in the model specification [1]. If matrix diffusion is only considered to penetrate up to $r=r_3$ then

$$\left.\frac{\partial C_{ox}^{R}(r,z,t)}{\partial r}\right|_{r=r_3} = 0. \tag{2.18}$$

The boundary conditions at the fracture are that the oxidant concentration is continuous at the interface of the bentonite and fracture, and that it is continuous at the interface of the rock and the fracture.

Also, the concentration is continuous across the bentonite to rock interface ($r=r_2$), and the evolution of the concentration at the interface may be computed by applying conservation of oxidant to obtain the appropriate

modification of the diffusion equation. The symmetry boundary condition in the rock is

$$\left.\begin{aligned} \frac{\partial C_{ox}^{R}(r,z,t)}{\partial z} &= 0, \\ \text{for } r > r_2 \text{ and } z &= Z. \end{aligned}\right\} \tag{2.19}$$

The initial condition in the rock is

$$C_{ox}^{R}(r,z,t{=}T_3) = 0. \tag{2.20}$$

In the fracture, the oxidant transport is modelled by an effective advection-diffusion equation, for the concentration $C_{ox}^{W}(r,t)$, in the form

$$\frac{\partial C_{ox}^{W}}{\partial t} = D_{ox}^{W}\frac{1}{r}\frac{\partial}{\partial r}(r\frac{\partial C_{ox}^{W}}{\partial r}) - \psi(r)\frac{\partial C_{ox}^{W}}{\partial r}\ , \tag{2.21}$$

where, following [3]

$$\psi(r) = \alpha v(1 - \frac{r_2^2}{r^2})\ , \tag{2.22}$$

v is the fracture flow speed, and α is a suitably chosen constant. The parameter set for this revised form of the model is therefore augmented by the triplet (D_{ox}^{W}, v, α).

2.5 Parameters of the Model

As far as possible, analysis of the problem described above is carried out for general values of the parameters. For the final results, we need to insert particular values and to quantify the effects of the uncertainty in various parameters. Also, in the course of the analysis, it is necessary to have some understanding of the parameter values, in order to see whether certain approximation techniques may be valid, and to define appropriate scales and e.g. grid sizes and time-scales for the numerical calculations.

A set of parameter values for the source term model is given, in final form in [7]. A subset of these values is required for the analysis of the redox front motion, and the values that were used in preliminary calculations are summarized in Table 4.

The possible range of values of a parameter $\mathcal{A}$, may be represented by a triplet of numbers $\mathcal{A} = (a_1, a_2, a_3)$, where a_2 denotes the best current estimate of the parameter, and a_1, a_3 are, respectively, lower and upper bounds for the values of the parameter. Thus, for example, the bentonite reductant capacity was represented by the triplet $Q^B = (0.05, 0.8, 2)\ keq.m^{-3}$.

For future reference we note that the quantity λ_1 defined by

$$\lambda_1 = \frac{\varepsilon^B r_1 F_{ox}}{2Q^B D^B_{ox}} \tag{2.23}$$

has typical values, in terms of the best estimates and ranges given by Table 4, corresponding to the triplet $\lambda_1 = (2 \times 10^{-6},\ 4 \times 10^{-3},\ 2)$. In equation 2.23, the values of the flux are estimated from volume production by the formula $F_{ox} = VG_{ox}/A$.

In the case of the oxidant production rate, a simple value, or range of values is inadequate as the production rate is a time-dependent function. The numbers presented for the best estimate and range indicate the orders of magnitude spanned by this function as t varies. The value of $G_{ox}(t)$ starts off at its upper value for small t and decays through the typical value, ultimately to zero, but, after about 1 million years, to about three orders of magnitude below its initial value. The analysis of oxidant production carried out by Christensen et al [20, 21, 22] has been used in this context before, [6], and serves as a useful basis for initial quantitative estimates. We may convert the data of [6] to the units used here.

For the purposes of computing the progress of the front, we need a representation of the production rate as a function of time. The available data gives the point values at certain times, together with the total production for the intervals with end-points at those times. In choosing an approximation, the critical quantity which must be preserved is the *integrated*

production rate, since it is this which determines the volume of oxidized bentonite and rock. This constraint can be satisfied by taking the production rate to be constant over each interval, the constant chosen so that the total production over each interval is correct.

Time ka	$G_{ox}(t)$ $keq.m^{-3}.(ka)^{-1}$
0.04 - 0.1	2.124
0.1 - 0.3	1.726
0.3 - 0.6	1.106
0.6 - 1	0.6858
1 - 10	0.3637
10 - 100	0.07965
100 - 1000	0.00774

Table 1: Piecewise constant representation of oxidant production rate

Table 1 represents the oxidant production rate, per unit volume, up to 10^6 years. For a canister failure at 10^6 years, which defines one set of base cases (Redox Front case RF1), in order to compute any significant front dynamics it is necessary to extrapolate beyond this point. Unfortunately the data to support such an extrapolation is rather sparse and we can only perform simple estimates.

Following discussions on the best method of proceeding [24, 25], the source of data was taken to be Figure 3-4 of [2]. This describes in graphical form the radioactivity in spent fuel. Next the key α-emitters predominating at one million years were identified (Ra-226 and Np-237). Then a crude empirical form for the decay rate of α production was established. In order to proceed further we also assume that the oxidant production rate is proportional to the α emission (there are no chemical back reactions). The production rate used was of the form

$$G_{ox}(t) = 0.00398(10^6/T)^{0.65} \ , 10^6 < T < 10^7$$

and was chosen to agree with the point production rate at 10^6 years (not the average for $10^5 - 10^6$), and to decay to between a fifth and a quarter of this value by 10^7 years.

In the definition of the preliminary base cases, further modulation of the oxidant production rate was applied, to describe the reaction of oxidants with the fuel. The rate of supply to the front is actually described by the replacement

$$G_{ox}(t) \longrightarrow \gamma G_{ox}(t)$$

where $1-\gamma$, $0 < \gamma < 1$ represents the proportion of the produced oxidants which react with the fuel.

For the remaining parameters, a subset of them is constant over the set of preliminary base cases. These are given by

- bentonite oxidant diffusivity $D_{ox}^{B} = 1.26m^2(ka)^{-1}$
- rock oxidant diffusivity $D_{ox}^{R} = 1.6 \times 10^{-3}m^2(ka)^{-1}$
- porosity of bentonite $\varepsilon^{B} = 0.35$
- porosity of rock $\varepsilon^{R} = 1.0 \times 10^{-3}$
- reductant capacity of rock $Q^{R} = 5.0 \times 10^{-2}keq.m^{-3}$
- interfracture spacing $Z = 0.5m$
- fracture half-width $b = 5.0 \times 10^{-5}m$
- canister porosity $\varepsilon^{C} = 0.01$
- water oxidant diffusivity $D_{ox}^{W} = 64m^2(ka)^{-1}$
- fracture advection factor $\alpha = 4$

Note that the fracture advection factor is taken to be 4, corresponding to one of the possible simplified advection models described in [5].

Front Case	T_1	Q^B	γ	Q^C	v
	years	$keq.m^{-3}$		$keq.m^{-3}$	$m.(ka)^{-1}$
RF1	10^6	0.4	0.5	0.0	10^5
RF2	10^5	0.4	0.5	0.0	10^5
RF3	10^4	0.4	0.5	0.0	10^5
RF4	10^3	0.4	0.5	0.0	10^3
RF7	10^3	0.4	0.9	27.385	10^3
RF8	10^3	0.4	0.9	0.0	10^3

Table 2: Base case definitions in terms of parameter values

The remaining parameters depend on the base case choice. The redox front base cases are labelled RF1 - RF8. Cases RF5 and RF6 require no calculations of the front, since in these cases all the oxidant is consumed by the fuel and/or canister. The parameters which vary with base case choice are the canister failure time T_1, the bentonite reductant capacity

Q^B (for which the default value is now $0.4keq.m^{-3}$), the oxidant escape factor γ, the fracture flow speed v and the canister reductant capacity Q^C. These parameters are associated with base case number according to table 2.

The bentonite capacity is represented explicitly in the table as it was originally proposed to vary it in case RF7, in order to contain the front within the buffer. With the associated canister capacity assumption of zero, this would have required an unphysical choice of Q^B. Following further discussions [25], it was decided to adjust the canister capacity (within the physical regime) instead. The value chosen is that shown in the table.

3 Methods of Solution

This section describes the various analytical and computational techniques used to solve the problem of the motion of the redox front.

3.1 Methodology

The approach adopted is to combine analytical and computational methods, with cross-verification where appropriate and possible. The initial portion of the problem, where the redox front is confined to the bentonite, is much more tractable analytically, and a variety of devices may be employed to extract information about the front. One of the cornerstones of the analysis is the so-called "quasi-steady-state" approximation (QSS), which is valid, essentially, when the reducing capacity of the bentonite is much greater than the capacity of the canister to supply oxidising species (in a sense which will be made precise shortly). This approximation (described, e.g. in [17]) has been used by Neretnieks [6] to obtain information about frontal motion, and was also used in [1] to obtain preliminary estimates in the present context. However, the uncertainty in the values of several of the parameters is such that the present problem might not be one for which the QSS approximation is valid. In particular, it will be seen that the validity of the QSS approximation is related to the size of the parameter λ_1 defined by equation 2.23, and that its validity requires $\lambda_1 << 1$. The best estimate satisfies this condition but the range of values does not. In order to avoid introducing further uncertainties from the use of this approximation when it need not be valid, we are led to seek improvements in this approximation, and indeed, to consider other limiting cases, and totally general formulations.

The analytical devices will be described in Section 3.2. In brief, there are four useful techniques. These are

- The exact solution available for a wire source ($r_1 = 0$) with constant flux;
- Conservation of oxidant;
- The quasi-steady-state approximation;
- An exact integral equation formulation, with asymptotic analysis.

The first three of these approaches are well known in one form or another. The integral equation approach is more novel, and may be approached

directly as a Laplace transform formulation or as the result of successive improvement of the quasi-steady-state approximation to an exact treatment. The latter approach is developed in Appendix A, and builds on the formulation of cylindrical problems given in [9, 10]. Appendix A also presents new results appropriate to the coupled problem involving the canister, and new results on the asymptotic forms of the solutions. These results are summarized in Section 3.2.

These approaches are complemented by a numerical scheme, which is used alone when the full problem, with the front in the rock-fracture system, is considered. It may also be used for the initial motion of the front in the bentonite, and this serves as a useful verification exercise for checking the numerical scheme and its computer implementation. The scheme was implemented as a FORTRAN program, and is based on the "Enthalpy method", proposed by Eyres *et al* [15], developed by Atthey [16], and described, for example by [17]. This method, as applied to diffusion and reaction in porous media, is outlined in Section 3.3. The verification of the resulting scheme is described in Section 4.

3.2 Analytical Methods

3.2.1 Exact Solution for a Constant Line Source

A problem for which an exact solution is available is that for the limiting case $r_1 = 0$, where the total flux out of the line source at $r = 0$ is some specified constant. The location of the front is known exactly as a function of time for this case. There are good reasons for presenting this case. First, we may consider this exact solution cut off for $r < r_1$, and examine its form in the exterior region $r \geq r_1$. In particular, the flux through this finite cylinder may be calculated as a function of time. In certain limiting cases, it is approximately constant. This may be used to infer properties of the solution to the real problem where a constant flux is specified on $r = r_1$. The second reason for considering this case is that we expect that for large times, when the front is at $r >> r_1$, the solution to the real problem should be close to that for the line source. Thus we may obtain estimates for little effort. These estimates may be bolstered by the exact formulation of the problem, and used to validate the computational model.

In this and subsequent Sections the time origin will be shifted so that the redox front is at r_1 at time $t = 0$ ($T_2 = 0$). Consider the function

$$C^B_{ox}(r,t) = C \int_{r/r^B_{ox}(t)}^{1} \frac{dx}{x} e^{-\lambda x^2}, \tag{3.1}$$

where

$$r_1^2 \leq r^2 \leq (r_{ox}^B(t))^2 = r_1^2 + 4\lambda \frac{D_{ox}^B}{\varepsilon^B} t, \tag{3.2}$$

and λ, C are to be determined. It may be verified that this function satisfies the diffusion equation (2.3) and it is clearly zero at the front. Furthermore, if the constant C is chosen as

$$C = 2\frac{Q^B}{\varepsilon^B}\lambda e^{\lambda}, \tag{3.3}$$

the condition (2.6) for the movement of the front is satisfied. The flux

$$F_{ox}(r,t) = -D_{ox}^B \frac{\partial C_{ox}^B}{\partial r}(r,t) \tag{3.4}$$

at any radius r is

$$F_{ox}(r,t) = \frac{2Q^B D_{ox}^B}{\varepsilon^B r}\lambda exp\{\lambda[1 - (r/r_{ox}^B(t))^2]\}. \tag{3.5}$$

This is independent of t only at $r = 0$, reflecting the fact that (3.1) is the exact solution for a constant line source. We are interested in the form of this function when $r = r_1$. The flux at time $t = 0$ is given by

$$F_{ox}(r_1,0) = \frac{2Q^B D_{ox}^B}{\varepsilon^B r_1}\lambda \tag{3.6}$$

and rises thereafter, approaching a value of this times e^{λ} as $t \longrightarrow \infty$. The scale of the variation is therefore governed by the size of λ, which is governed by (3.6). The time-scale τ for the variation may be identified as the time at which the two terms on the right side of (3.2) are equal, and is therefore

$$\tau = \frac{Q^B r_1}{2F_{ox}(r_1,0)}. \tag{3.7}$$

For times $t << \tau$ the flux attains the lower value, while for $t >> \tau$ it attains the upper value. This characteristic time-scale plays a role in subsequent considerations also.

The right way to use these results in the problem at hand is to turn the problem around and consider what happens if we supply a constant flux at either of the two limiting values. If we supply a constant flux at the lower (initial) value, the front will initially (i.e., for $t << \tau$) move at the rate given by λ from (3.6), but will slow down as the flux becomes insufficent to sustain the motion. On the other hand, if we were to supply constant flux at the higher (ultimate) value, the front will move at a faster rate than that implied by (3.2). (In some asymptotic sense the front given by (3.2) might be expected to 'catch up' for large times.) With one further

shift in viewpoint results about the problem where the flux has a single fixed value F_{ox} may be inferred. We consider two values of λ. The first corresponds to a problem where our constant flux is the initial flux; the second to the problem where it is the final flux. These two values are the roots λ_1 and λ_2 respectively of the equation

$$\lambda_1 = \frac{\varepsilon^B r_1 F_{ox}}{2Q^B D^B} = \lambda_2 exp\{\lambda_2\}. \tag{3.8}$$

We may deduce from these considerations that if the flux is constant the front location satisfies the inequalities

$$4\lambda_2 \kappa^B t < r_{ox}^B(t)^2 - r_1^2 < 4\lambda_1 \kappa^B t, \tag{3.9}$$

where the effective diffusivity $\kappa^B = D^B/\varepsilon^B$. We expect that initially the front is close to the upper value, with near equality for times much less than τ. At late times we expect the front location to be closer to the lower value, in some suitable asymptotic sense, if the front remains in the bentonite. These remarks may be made more precise and justified by use of the integral equation formalism.

Note that if $\lambda_1 << 1$ the front location is constrained to lie within a narrow region, since λ_2 is then only slightly smaller than λ_1. The bounds on the front location are less tight for moderate to large values of λ_1. This will be illustrated in Section 4.

3.2.2 Conservation of Oxidant

A simple and useful relation may be obtained by writing down the integral equations which express conservation of oxidant. Since

Oxidant supplied at r_1 =

Oxidant reduced + Total in Distribution

we deduce the relation:

$$2\pi r_1 \int_0^t dT F_{ox}(T) = \pi Q^B [r_{ox}^B(t)^2 - r_1^2] + 2\pi\varepsilon^B \int_{r_1}^{r_{ox}^B(t)} r dr C_{ox}^B(r,t) \tag{3.10}$$

Use of conservation of oxidant in this integral form is sometimes more useful than the corresponding differential form. Note that for any guess at the form of the oxidant distribution, it supplies an equation for the location of the front. The form of this relation to some extent explains the behaviour of the solution for large Q^B and/or small times. If we assume that the amount of oxidant reduced is much greater than that in

the distribution behind the front, so that the first term on the right side of this equation dominates, the front is seen to attain the upper bound of (3.9).

In a similar way, an integral conservation law including canister effects can be given. If the time origin is shifted to the point at which the reducing capacity of the canister is exhausted, then the following conservation law holds:

$$\pi r_1^2 \int_0^t G_{ox}(T)dT =$$

$$\pi Q^B[r_{ox}^B(t)^2 - r_1^2] + 2\pi\varepsilon^B \int_{r_1}^{r_{ox}^B(t)} drrC_{ox}^B(r,t) + \varepsilon^C \pi r_1^2 C_{ox}^B(r_1,t). \quad (3.11)$$

3.2.3 The Quasi-Steady-State Approximation

In order to sharpen further the understanding of the properties of the solution, it is useful to introduce an *ansatz* for the form of the solution which is expected to be accurate in certain limiting conditions. If the bentonite has a high Q^B in relation to the oxidant production rate, the front will move slowly and near steady-state conditions will exist behind the front. The concentration of oxidant therefore satisfies Laplace's equation approximately. Given that it vanishes at the front, it must therefore be of the form

$$C_{ox}^B(r,t) = \mu(t) ln[r_{ox}^B(t)/r], \quad (3.12)$$

for some function $\mu(t)$. What we take for μ depends on how this guess at the distribution is to be used. We may put a constraint on μ by imposing either of the boundary conditions (2.6) or (2.7/8), or one of these conditions could be replaced by the integral law for conservation given by (3.10/11). Consider imposition of (2.7), the flux boundary condition. Clearly

$$\mu(t) = \frac{r_1 F_{ox}(t)}{D_{ox}^B} \quad (3.12)$$

We may then substitute in one of the other constraints and deduce a condition on the front location. The result may be expressed in several ways. Our immediate purpose here is to illuminate the remarks made concerning the consequences of the available exact solution for a wire source, and it will suffice to consider constant flux. For small λ_1 (when we expect the quasi-steady-state technique to be reasonable), if we use the integral constraint (3.10) the front location is given by

$$r_{ox}^B(t)^2 - r_1^2 = 4\kappa^B\{\lambda_1 t + \lambda_1^2 \tau[ln(1+\frac{t}{\tau}) - \frac{t}{\tau}]\}. \quad (3.14)$$

If we had merely used the frontal boundary condition (2.7) only the first term would have been found. For times $t << \tau$, we have

$$r_{ox}^B(t)^2 - r_1^2 = 4\kappa^B \lambda_1 t + O(t^2), \tag{3.15}$$

whereas the behaviour for large times is given by writing (3.14) in the form

$$r_{ox}^B(t)^2 - r_1^2 = 4\kappa^B[\lambda_1 - \lambda_1^2]t + o(t)\ , \quad t \longrightarrow \infty. \tag{3.16}$$

Thus for small times the solution is indeed close to the upper bound of (3.9). For large times, if we note that the solution for small λ_1 of the equation $\lambda_2 exp(\lambda_2) = \lambda_1$ is $\lambda_2 = \lambda_1 - \lambda_1^2 + O(\lambda_1^3)$, it becomes clear that the lower bound is approached logarithmically (i.e., we could replace the $<$ in (5.9) by a $\sim$).

Equation (3.14) gives the second order corrections to the front location beyond those given in Appendix 1 of [1]. As many higher order corrections as desired could, in principle, be computed by using the quasi-steady-state form as the basis for a perturbation analysis. For large values of λ_1, however, questions of convergence arise, or many terms may be needed for accuracy. What is needed is a device for summing the perturbation series, in some useful sense, and working with relations exact for all values of λ_1.

Analogous relations may be written down incorporating canister effects. We will note the "near QSS" equation for arbitary volume production rate. With a quasi-steady-state profile chosen to satisfy the conditions at the front

$$C_{ox}^B = \frac{Q^B}{4D^B}\rho ln(\rho/r^2) \tag{3.17}$$

we may deduce a first order equation of motion for the front. For the case of general oxidant production, we obtain

$$\frac{r_1^2}{Q^B}\int_0^t G_{ox}(T)dT = (\rho - r_1^2)(1 + \frac{\dot{\rho}}{4\kappa^B}) + (\varepsilon^C - \varepsilon^B)\frac{r_1^2}{4D^B}\rho ln(\frac{\rho}{r_1^2}) \tag{3.18}$$

It may be verified that this has the correct small time behaviour. Moreover, with non-zero decay of the oxidant production rates, the large time behaviour should be correct for all values of the parameters, since ultimately QSS conditions *will* apply.

3.2.4 Integral Equation Formulation

The exact formulation of the problem has as its roots the "quasi-steady-state" approximation discussed above, though it may be alternatively derived by a direct Laplace transform of the entire problem. The direct

Laplace transform route involves some subtle analytical questions, as discussed in e.g. [13] for the linear problem, and the method based on improving the QSS formulation is in some ways more transparent. The idea is to use the QSS formulation as the first term in a perturbation series expansion. This leads to an *infinite-order* differential equation for the front. However, the series can in fact be summed when Laplace-transformed, and leads to an integral equation for the front alone, i.e., decoupled from the oxidant concentration. This was done in the linear case in [12], and the basic framework pertinent to the cylindrical case is presented in [9, 10]. Integral equations may be written down for several cases, including the simplest situation where the concentration is prescribed on $r = r_1$. Here the results for prescribed flux $F_{ox}(t)$ or oxidant production rate $G_{ox}(t)$ will be given. Let the Laplace transforms of these quantities be denoted by $\bar{F}_{ox}(p)$, $\bar{G}_{ox}(p)$ respectively. It is also convenient to describe the front location by a relation inverse to $r = r_{ox}^B(t)$, i.e. $t = f(r)$, and to introduce the ultimate location of the front as R ($R = r_{ox}^B(\infty)$, and is possibly infinite. We also define

$$q = \sqrt{\frac{p}{\kappa^B}} \tag{3.19}$$

It is shown in Appendix A that the following integral equations hold. With a flux boundary condition, we have:

$$\bar{F}_{ox}(p) = Q^B \int_{r_1}^{R} dx x e^{-pf(x)} q[K_1(qr_1)I_0(qx) + I_1(qr_1)K_0(qx)]. \tag{3.20}$$

and the boundary condition for the full coupled problem takes the form

$$\bar{G}_{ox}(p) = Q^B \int_{r_1}^{R} dx x e^{-pf(x)} q^2[\hat{K}(qr_1)I_0(qx) - \hat{I}(qr_1)K_0(qx)]. \tag{3.21}$$

where $\hat{K} = K_2 + \delta.K_0$, $\hat{I} = I_2 + \delta.I_0$, and $\delta = \varepsilon^C/\varepsilon^B - 1$.

3.2.5 Remarks

1. The I_i, K_i are modified Bessel functions (see, e.g. [18]).

2. These integral equations could have been derived by a direct Laplace transform method.

3. They are linear in the flux or oxidant production rate.

4. We may consider their application for all values of the relevant parameters. There is no longer any constraint, for example that Q^B be large compared to other quantities. As was the case in the example, the front motion depends in the general case only on the ratio of the flux to the bentonite reduction capability.

5. The coupled problem, and those where the concentration or flux are specified, on $r = r_1$, differ only in the choice of kernel in the integral equation.

3.2.6 Simple Consequences

The integral equations contain all the information about the front motion once the left sides of (3.20/21) have been specified. It is difficult to find exact solutions, but it may be verified, for example, that (3.20) produces the correct front motion for a line source ($r_1 = 0$).

Further results may be derived by considering extreme values of the transform variables p or $q = \sqrt{(p/\kappa^B)}$. First, if we set $q = p = 0$, we may deduce the ultimate location of the front, given by R. We only expect this to be finite if $\bar{F}_{ox}(0)$ (with (3.20)) or $\bar{G}_{ox}$ (with (3.21)) exist, these quantities being the total oxidant flux/production integrated over all time. The extraction of these limits requires the appropriate expansion of the Bessel function kernels. When this is done, (3.20) yields

$$Q^B(R^2 - r_1^2) = 2r_1\bar{F}_{ox}(0). \tag{3.22}$$

and (3.21) yields

$$Q^B(R^2 - r_1^2) = r_1^2\bar{G}_{ox}(0). \tag{3.23}$$

These relations are consistent with the conservation of oxidant, expressed by (3.10/11), when it is appreciated that the ultimate (and steady-state) concentration distribution is zero. (If the front comes to a halt, use of the boundary conditions and Laplace's equation implies zero concentration everywhere.)

3.2.7 Asymptotic Forms

In Appendix A.2 it is shown that, in terms of the parameters introduced previously, the resulting solution for the front is of the form

$$\frac{4\kappa^B t}{r_1^2} = \frac{1}{\lambda_1}(\frac{r^2}{r_1^2} - 1) + 2(\frac{r}{r_1} - 1)^2 - \frac{2}{3}(\frac{r}{r_1} - 1)^3 + O((r/r_1 - 1)^4)) \tag{3.24}$$

for small $|r - r_1|$. Writing $r = r_{ox}^B(t)$, this may be inverted to give

$$r_{ox}^B(t)^2 - r_1^2 = 4\kappa^B\lambda_1 t\{1 - \frac{\lambda_1 t}{2\tau} + \frac{\lambda_1^2 t^2}{2\tau^2}(1 + 2/\lambda_1)\} + O(t^4). \tag{3.25}$$

This gives the solution for general values of the parameters, for small values of t. We note that the first 2 terms are consistent with (3.14),

derived on the basis of the steady state approximation. The form of the expansion suggests that it gives reasonable answers for the front location provided the quantity $\frac{\lambda_1 t}{\tau}$ is small.

When the front is a long way out, an asymptotic treatment (given in Appendix A.2) may be applied. The final result may be best expressed in forms analogous to (3.24) and (3.23). We have, respectively

$$\frac{4\kappa^B t}{r_1^2} \sim \frac{1}{\lambda_2}\frac{x^2}{r_1^2} - 2ln(\frac{x}{r_1}), \quad x \longrightarrow \infty \tag{3.26}$$

and inverse form

$$r_{ox}^B(t)^2 - r_1^2 \sim 4\kappa^B \lambda_2 t\{t + \lambda_1 \tau ln(t/\tau)\}, \quad t \longrightarrow \infty. \tag{3.27}$$

It may be verified that for small λ_1, this agrees with (3.14) to order λ_1^2 for large t.

When canister effects are included use of (3.21) and asymptotic methods may be used to extract corresponding estimates in terms of the volume oxidant production rate. If we write, for small times,

$$r_{ox}^B(t)^2 - r_1^2 \sim 4\kappa^B \mu t, \tag{3.28}$$

then μ is determined by

$$\mu + \frac{\varepsilon^C}{\varepsilon^B}\mu^2 = \frac{r_1^2 G_0}{4\kappa^B Q^B} \tag{3.29}$$

where G_0 is the oxidant production rate at time zero. If the oxidant production remains constant or subsequently decays, this equation may be considered as supplying an upper bound for the front velocity and location. The effect of the canister is to slow the front, and we note that if $\varepsilon^B = \varepsilon^C$, this effect may be regarded as taking the initial motion closer to that for the exact solution for a wire source.

Another useful limiting case is obtained by considering the production decay times to be long compared with the times of interest in the front motion. If the oxidant production is set to a constant, the analogue of (3.26) may be obtained as

$$\frac{4\kappa^B t}{r_1^2} \sim \frac{1}{\Lambda_2}\frac{r^2}{r_1^2} - 2(1 - \varepsilon^C/\varepsilon^B)ln(r/r_1) + O(1) \tag{3.30}$$

where

$$\Lambda_2 exp\Lambda_2 = \frac{r_1^2 G_0}{4\kappa^B Q^B} \tag{3.31}$$

Here the effect of the canister is to modulate the size of the log term. If the two porosities are equal, the log term is zero, and the solution is very close to the exact solution for a wire with an equivalent production rate.

3.3 Numerical Methods

When the front reaches the rock-fracture system the problem becomes more difficult and, in the absence of sufficiently powerful analytical techniques, a numerical scheme is employed. The scheme used is the "enthalpy method", and the particular approach is that described, e.g. in [17]. This method is outlined in brief here, with the intention of making it clear precisely what form of the enthalpy function is appropriate to this problem. For simplicity, the description here will focus on a homogeneous problem, such as exists in the bentonite. Indeed, the inital motion of the front through the bentonite may be solved by this method, and a comparison of the results with those obtained from the analytical treatment above is a useful cross-verification exercise which ensures the integrity of the computer program. The verification is described in Section 4.

The bentonite enthalpy $H^B(r,t)$ is defined by

$$H^B(r,t) = \varepsilon^B C^B_{ox}(r,t) + Q^B\theta(C^B_{ox}(r,t)) \tag{3.32}$$

where $\theta(x)$ is the step function satisfying

$$\theta(x) = \begin{cases} 1, & \text{if } x > 0; \\ 0, & \text{if } x < 0. \end{cases} \tag{3.33}$$

This has the property that it satisfies a modification of the diffusion equation on a region containing both sides of the front. In fact:

$$\frac{\partial H^B}{\partial t} = D^B_{ox}\nabla^2 C^B_{ox}(r,t) : \quad r_1 < r < r_2. \tag{3.34}$$

This can be made the basis of a straightforward *explicit* time-stepping algorithm. At each time-step the following operations are carried out:

- The current value of H^B is updated according to (3.34);
- The value of $C^B_{ox}(r,t)$ is updated according to the relation inverse to (3.32);
- The boundary conditions are applied.

At each stage the location of the front may be identified as the value of r, say r_0, at which a discontinuity in the enthalpy of size Q^B is encountered, and in addition, the concentration is zero for $r > r_0$. The extension to multi-dimensional problems is reasonably straightforward. (Implicit schemes are also possible, but their implementation requires extra processing to circumvent the difficulty of deciding in advance where the front

will be at the next time step.) In order to get a good estimate of the front behaviour near the fracture, and to account for the uncertainty in the fracture width, a variable grid size was employed, with finer steps near the fracture.

In the implementation of this approach as applied to the present problem there are two distinct phases. The first phase constitutes the 1-dimensional radial motion through the bentonite. The computer model (having been verified against analysis for a wide range of parameter values) inspects the value of λ_1 for the bentonite and, if $\lambda_1 < 0.1$, discards the enthalpy algorithm and substitutes an expression for the front such as (3.14) or (3.18) (as appropriate). When the front is in the rock-fracture region, the enthalpy method is employed in the rock region, with a 2-dimensional numerical diffusion algorithm applied in the bentonite region.

The rock enthalpy function is given by

$$H^R(r,t) = \varepsilon^R C^R_{ox}(r,z,t) + Q^R\theta(C^R_{ox}(r,z,t)) \tag{3.35}$$

and satisfies

$$\frac{\partial H^R}{\partial t} = D^R_{ox}\nabla^2 C^R_{ox}(r,z,t) \tag{3.36}$$

for $r > r_2$ and $b < z < Z$.

4 Verification

The analytical methods described in Section three produce several simple constraints, for the radial motion through the bentonite, which may be used to verify the numerical schemes. From the exact solution for a wire bounds were inferred for the solution of the problem for constant flux. For the case of either constant flux or constant volume production the integral equation method led to asymptotic estimates valid for small or large times. The large time estimates are useful since, although in reality the front will no longer be in the bentonite at late times, one can get a feel for the overall accuracy of the program, after many time steps, by considering the problem where the bentonite extends from r_1 to infinity, and verifying that the numerical solution is close to the exact analytical asymptote. Finally, when the parameters are such that a quasi-stationary method is reasonable, comparison with results such as (3.14) are possible.

Figures 2 to 4 show the results of the verification for the case of constant flux. For verification purposes the fluxes were taken to be such as to produce a problem which was nearly quasi-stationary (Figure 2), and then fluxes of ten (Figure 3) and one hundred (Figure 4) times this value were considered. It should be noted that the value of λ_1 associated with Figure 3 is the same order of magnitude as the largest that would be experienced in the real problem under consideration. In each of these figures the stepped curve shows the numerical solution. The stepping is the result of the spatial discretization. The horizontal axis denotes time, and the vertical axis represents the quantity $r_{ox}^B(t)^2 - r_1^2$. Also, in each of these figures there are two bold straight lines. These are the bounds on the solution given by equation (3.9), and it is clear that the numerical solution lies within these bounds. The upper bound is what is predicted by the quasi-stationary limit, (without correction by the integral conservation equations) and may be a significant over-estimate.

Figure 2 shows some additional comparisons. The small-time asymptote (3.25) from the integral equation method is shown to quadratic order, as is the corrected quasi-stationary solution (3.14), which may also be regarded as an interpolation from the late-time formula (3.27). Good agreement is obtained.

Figure 4 shows the results after many time steps for a large value of λ_1. The additional bold curve directly above the stepped numerical solution is the late-time asymptote (3.27), and shows the small accumulated effect of discretization errors after many thousands of time steps. The near-vertical line in this Figure is the quasi-stationary curve, and illustrates the danger in applying this approximation scheme for values of $\lambda_1 >> 1$.

One can make similar comparisons for the more realistic case of volume oxidant production. One of the cases used to verify this part of the algorithm is illustrated by Figure 5. This corresponds to the same input data as represented by Figure 3, but with a finer radial grid employed for the numerical calculations. The rate of volume production is taken to be the constant value which, in the limit of zero can porosity, would produce the same constant flux as produced in Figure 3. However, in this case, the can porosity ε^C and the bentonite porosity ε^B are equal. The asymptotic lines computed from the integral equations are shown in Figure 5, together with the enthalpy solution for volume production and the corresponding solution for a flux boundary condition. The numerical solution is consistent with all the assertions made in Section 3.2. In particular, the parameter μ given by equation (3.29) does indeed supply an upper bound and a plausible small-time asymptote, while the parameter Λ_2 computed from equation (3.31) supplies a lower bound and a plausible late-time asymptote. As expected, the inclusion of canister effects, even before we consider the absorption of oxidants within the canister, does indeed slow down the front.

The numerical scheme as implemented therefore provides good agreement with the analytical results, and may be used with some confidence in the more general, 2-dimensional problem. The full problem will be considered in the next Section.

5 Applications

5.1 Qualitative Behaviour of Redox Front

The behaviour of the front in the bentonite has been discussed in Sections 3 and 4, where the analytical and computational results are established and verified. The quantitative results associated with this stage of the process will be discussed in Section 5.2.

The qualitative behaviour of the front for the full problem, with the original "zero-concentration" boundary condition at the fracture, is shown in Figure 7, which has been calculated for an unrealistic case where the rock and bentonite have the same diffusivity and reductant parameters, and where the fracture is considerably wider than normal. This case is presented to illustrate the effects of the fracture in isolation from the effects of the change of properties of the media. The front profile is shown for a sequence of equally-spaced times. It is clear that away from the fracture the front carries on as if the fracture were absent, for some time. The front is *retarded* near the fracture, and the retardation effect gradually spreads up from the fracture. This situation has received comment from many sources, to the effect that it is not what was expected on physical grounds, and that the transport effects of the fracture should produce advancement along the fracture, rather than retardation.

With the inclusion of the modified fracture model, the qualitative behaviour seems to be more in accordance with what was expected. Figure 8 shows a typical concentration profile shortly after the front escapes the bentonite. This figure is for realistic parameter values. The front is clearly advanced by the fracture. Another feature to note is the sharp change in slope at the bentonite-rock interface. Flux continuity, together with the large change in diffusivity between the bentonite and rock, require that the radial derivative of the concentration change quite markedly at the interface, as is shown in the figure.

5.2 Quantitative Results

A discussion of the importance of the canister and bentonite reductant capacities on the front behaviour was given in the first report on this work [3]. Here the base case results will be summarized. The detailed output of the calculations consists of a table of "switch times", consisting of the times at which cells in the grid employed for numerical solution switch from being reducing to oxidizing. This table is generated for each base case, and fed into the radionuclide transport calculations.

Some remarks about the operation of the code for the base cases are pertinent. For the parameter values associated with the base case, the motion within the bentonite can be described by "quasi-stationary" methods, and the code automatically switched to the use of a numerical form of equation (3.18), (physically, the QSS approximation improved by the application of the integral conservation law). When the rock is reached, the enthalpy method takes over for the computation of the two-dimensional dynamics of the front, which evolves from its symmetric form to the shaped profile shown in figure 7. In each base case the computation was carried out for as long as was practical.

The most usefully surveyable results consist of the summary information about the progress of the front. This is summarized in the following table. In the table T^C_{esc} denotes that time at which the front escapes the canister, and T^B_{esc} denotes the time at which the front reaches the rock/fracture. All times are in years.

Front Case	T_1	T^C_{esc}	T^B_{esc}
RF1	10^6	10^6	1.57×10^6
RF2	10^5	10^5	3.5×10^5
RF3	10^4	10^4	3.4×10^4
RF4	10^3	10^3	6.35×10^3
RF7	10^3	8.8×10^6	$> 10^7$
RF8	10^3	10^3	4×10^3

Table 3: Base cases: summary of front evolution

6 Conclusions

A model has been developed which is capable of solving the major part of the problem posed in [1] for the motion of a redox front through a system of bentonite and fractured rock.

The solution procedure requires no approximations beyond the idealizations made in the original specification of the model, and is therefore capable of describing the front motion when more traditional techniques, such as quasi-steady-state methods, may be inappropriate.

The method of solution has been validated against analytical results, from several different approaches, on the initial cylindrical problem where the front moves radially through the bentonite. The application of the integral equation technique to the problem of redox front motion appears to be new, and it may find other applications within this general area, in situations which are, or may be idealized as, sufficiently symmetric for such a 1-dimensional treatment. It would be useful to devise alternative numerical schemes for direct solution of the integral equations, which fall into a category of equations for which general numerical schemes are not, at present, readily available.

The model could be made more detailed through the inclusion of canister end effects and irregular fluxes at the canister wall, with only slight modifications to the numerical schemes. It would, however, require a significant increase in computation to cope with such a fully 3-dimensional problem. A more useful enhancement would be the ability to model the fracture in more detail, including the possible creation of a front in the fracture, due to the presence of reducing agents.

In addition, it would be useful for further verification to be performed. The basic method has been thoroughly tested for the 1-dimensional component of the motion, corresponding to the motion of the front through the bentonite. It would be useful to adjoin to this some further analytical treatment of the 2-dimensional problem, preferably applicable for quite general parameter values.

The capacities of the canister materials and the bentonite to absorb oxidants requires further careful scrutiny, as simple estimates have indicated that the front may be trapped in the canister, trapped in the bentonite, or progress into the rock-fracture system, depending on whether these capacities are at the lower or higher end of their present estimated ranges. The capacity of the fuel to absorb oxidants is also important here. These points are well illustrated by the behaviour for each of the base cases: significant progression of the front into the rock always depends on having

a low canister capacity, and a moderate to high capacity can result in the front being trapped in the canister or bentonite, at least on timescales less than 10 million years.

It is clear that the more realistic treatment of the fracture presented in this present study has made a qualitative change to the behaviour of the front in the neighbourhood of the fracture. This suggests that the previous zero-concentration condition, corresponding to very high flow rates in the fracture, may be inappropriate. Further study of the fracture is required. In particular, the influence of reducing agents in the fracture water should be studied, and this is under consideration.

In summary, a methodology has been developed for the calculation of the motion of the front, without restrictions on input parameter values, and appropriate data may be output to the stage of the modelling describing radionuclide transport.

It is further suggested that the techniques employed here, in particular, the enthalpy method, may also be useful in other problems of frontal motion of relevance to radionuclide transport, such as those which arise in the study of natural analogues.

A Appendix: Mathematical Details

A.1 Derivation of Integral Equations

In this Appendix the mathematical details of the arguments leading to an integral equation for the front motion are summarized. The discussion given here builds on that given by Dewynne & Hill [9, 10] for a cylindrical geometry (see also [13] for a discussion of the corresponding one-dimensional problem). There are good reasons for going into some detail on these techniques. Problems of front motion are of increasing interest in radionuclide migration problems, due to the high sensitivity of the solubility of many radionuclides to the redox potential. The problems of interest may not always be of a type where the quasi-steady-state approximation is appropriate. In such cases, one is led to consider alternatives. The integral equation technique is useful in problems where it is possible to reduce the Laplace operator to a 1-dimensional operator. This includes 1-dimensional problems, and problems with cylindrical or spherical symmetry. It also includes radial problems with non-integral dimension, which may be useful as a classical approach to geometries of a fractal nature. Although it is restricted in application to such geometries, it is particularly useful since there are no restrictions on the other parameters of the problems, and it decouples the motion of the front from the problem of finding the concentration behind the front. It may also be useful in problems where an approximate symmetry exists. Finally, it is useful to have analytical estimates for special cases, with which to verify computer codes developed for solving frontal motion problems. Throughout this Appendix we consider a front motion problem on the region $r > r_1$.

It is convenient to formulate the equations for the front in terms of Laplace transforms. This may be done by a direct route (as, for example, was done by [13], for the one-dimensional case). It will be useful to take a slightly more circuitous route which explains the role of the QSS approximation and makes the analysis somewhat more transparent. The corresponding derivation in the linear case is given by [12]. The Laplace transform of the flux is

$$\bar{F}_{ox}(p) = \int_0^\infty dt \epsilon^{-pt} F_{ox}(t). \qquad (A.1)$$

Transforms of the other quantities are similarly defined. The flux boundary condition is therefore

$$D_{ox}^B \frac{\partial \bar{C}_{ox}^B}{\partial r}(r_1, p) = -\bar{F}_{ox}(p) \qquad (A.2)$$

For the coupled problem, we have

$$\varepsilon^C p\bar{C}^C_{ox}(p) = \bar{G}_{ox}(p) - \frac{A}{V}\bar{F}_{ox}(p) \tag{A.3}$$

$$\bar{C}^C_{ox}(p) = \bar{C}^B_{ox}(r_1, p) \tag{A.4}$$

The boundary condition in terms of the bentonite concentration alone is therefore

$$\frac{\varepsilon^C}{\varepsilon^B}q^2\bar{C}^B_{ox}(r_1, p) - \frac{2}{r_1}\frac{\partial\bar{C}^B_{ox}}{\partial r}(r_1, p) = \frac{1}{D^B_{ox}}\bar{G}_{ox}(p). \tag{A.5}$$

We proceed by using the QSS approximation as the first term in a series expansion. Explicitly, let

$$C^B_{ox} = \frac{Q^B}{4D^B_{ox}}\sum_{n=0}^{\infty} C_n \tag{A.6}$$

where

$$C_0 = \rho ln[\frac{\rho(t)}{r^2}]. \tag{A.7}$$

$$\rho(t) = [r^B_{ox}(t)]^2. \tag{A.8}$$

Here we arrange that the equation of motion for the front is satisfied by C_0 alone. A sufficient condition for A.6 to give a solution of the diffusion equation is that

$$\nabla^2 C_i = \frac{1}{\kappa^B}\dot{C}_{i-1}, \tag{A.9}$$

and the boundary conditions at the front will be satisfied if for all $i \geq 1$:

$$C_i = 0 = \frac{\partial C_i}{\partial r} \tag{A.10}$$

at $r = r^B_{ox}(t)$. Clearly we may solve these by repeated differentiation with respect to time and double integration in the radial variable r. Let I denote the operation on functions given by

$$I[f](r,t) = \int_r^{r^B_{ox}(t)} \frac{dr'}{r'}\int_{r'}^{r^B_{ox}(t)} r''dr'' f(r'', t), \tag{A.11}$$

Then we have

$$C_n = \frac{1}{\kappa^B}I\dot{C}_{n-1} \tag{A.12}$$

and furthermore

$$C_n = \frac{1}{\kappa^B}\frac{\partial}{\partial t}IC_{n-1}, \tag{A.13}$$

since we arrange that at each stage of the integration we preserve the condition that the function vanishes at the front. By iterating these relations, we deduce that

$$C_n = (\frac{1}{\kappa^B})^n(\frac{\partial}{\partial t})^n I^n C_0. \tag{A.14}$$

Writing $\psi^n = I^n C_0$, we can write the bentonite concentration as

$$C^B_{ox}(r,t) = \frac{Q^B}{4D^B_{ox}} \sum_{n=0}^{\infty} (\frac{1}{\kappa^B})^n (\frac{\partial}{\partial t})^n \psi_n, \tag{A.15}$$

where

$$\psi_0 = C_0, \quad \nabla^2 \psi_n = \psi_{n-1}, \psi_n = I\psi_{n-1}. \tag{A.16}$$

The first few ψ_n may be obtained straightforwardly by direct integration, and there is a pattern, as n varies, which suggests that some general expression exists. The appropriate expression is best found through the introduction of a suitable generating function. Let

$$\Psi(r,t) = \sum_{n=0}^{\infty} \lambda^n \psi_n. \tag{A.17}$$

Evidently

$$\nabla^2 \Psi = \lambda \Psi. \tag{A.18}$$

Furthermore Ψ satisfies the boundary conditions at the front. It may be written down as the appropriate solution of Bessel's equation:

$$\Psi = 2\dot{\rho}\{K_0[\sqrt{\lambda}r]I_0[\sqrt{\lambda}r^B_{ox}(t)] - I_0[\sqrt{\lambda}r]K_0[\sqrt{\lambda}r^B_{ox}(t)]\}. \tag{A.19}$$

This manifestly vanishes at the front, and its derivative obeys the appropriate front movement condition by virtue of a Wronskian identity for Bessel functions. If desired, the ψ_n may be found by expansion of (A.19) in the form of (A.17).

The direct use of these relations leads to an infinite-order differential equation for the front, obtained by substitution of the series solution (A.15) in the remaining boundary condition at $r = r_1$. A more convenient form for the boundary condition is obtained by the use of the Laplace transform. The point is that the time-derivatives in (A.15) become powers of the transform variable, and the series may then be summed through the generating function, provided certain initial conditions apply to the ψ_n, namely that their first $n-1$ time derivatives vanish. A sufficient condition for this to be the case is that all the time derivatives of the function $\rho(t)$ are bounded as $t \longrightarrow 0$. We will make this assumption for the finite cylinder. In this case we have

$$\bar{C}^B_{ox}(r_1,p) = \frac{Q^B}{4D^B_{ox}} \int_0^{\infty} dt e^{-pt} \dot{\rho} \sum_{n=0}^{\infty} (p/\kappa^B)^n \psi_n[r_1, r^B_{ox}(t)]. \tag{A.20}$$

For the problems of interest, it may be assumed that the front location is a monotone function of time. In this case we may change variable to $x = r^B_{ox}(t)$, and let $f(x)$ denote the time at which the front is at x. At

time zero, $x = r_1$, and as $t \longrightarrow \infty$, $x \longrightarrow R$, where possibly $R = \infty$. With this change of variable:

$$C^B_{ox}(r_1, p) = \frac{Q^B}{2D^B_{ox}} \int_{r_1}^{R} dx x e^{-pf(x)} \sum_{n=0}^{\infty} (p/\kappa^B)^n \psi_n(r_1, x). \qquad (A.21)$$

By use of the generating function, and setting $q = \sqrt{p/\kappa^B}$ as before, the concentration at $r = r_1$ may be written in terms of the front as

$$D^B_{ox}\bar{C}^B_{ox}(r_1, p) = Q^B \int_{r_1}^{R} dx x e^{-pf(x)} [K_0(qr_1)I_0(qx) - I_0(qr_1)K_0(qx)]. \qquad (A.22)$$

By similar arguments the flux boundary condition at $r = r_1$ becomes

$$\bar{F}_{ox}(p) = Q^B \int_{r_1}^{R} dx x e^{-pf(x)} q [K_1(qr_1)I_0(qx) + I_1(qr_1)K_0(qx)]. \qquad (A.23)$$

and the boundary condition for the full coupled problem takes the form

$$\bar{G}_{ox}(p) = Q^B \int_{r_1}^{R} dx x e^{-pf(x)} q^2 [\hat{K}(qr_1)I_0(qx) - \hat{I}(qr_1)K_0(qx)]. \qquad (A.24)$$

where $\hat{K} = K_2 + \delta . K_0$, $\hat{I} = I_2 + \delta . I_0$, and $\delta = \varepsilon^C/\varepsilon^B - 1$.

A.2 Derivation of Asymptotic Forms

More detailed information about the front location may be obtained by considering the integral equations for other limiting values of p.

A.2.1 Flux Boundary Condition: Small Times

For the case of flux boundary conditions, we may write

$$\bar{F}_{ox}(p) \sim \frac{F}{p}, p \longrightarrow \infty, \qquad (A.25)$$

where F is the flux at time $t = 0$, and this relation is *exact* if the flux is constant. Similarly,

$$\bar{G}_{ox}(p) \sim \frac{G}{p}, . p \longrightarrow \infty. \qquad (A.26)$$

where G is the oxidant production rate at time $t = 0$.

Consider first the constant flux problem. Since $f(r_1) = 0$ and f is monotone increasing with r, with $f'(0) > 0$ suggested by our previous approximations, as $p \longrightarrow \infty$ the decay of the exponential containing $f(x)$ is

stronger than the growth of the Bessel functions except near $x = r_1$, so the dominant contribution to the integral comes from this neighbourhood. In a neighbourhood of $x = r_1$, the Bessel function kernel $W = q[K_1(qr_1)I_0..]$ may be expanded as

$$W \sim \frac{1}{r_1}\{1 + \frac{p}{\kappa^B}w(x) + O((x - r_1)^4)\}, \qquad (A.27)$$

where

$$w(x) = \frac{1}{2}(x - r_1)^2 - \frac{1}{6r_1}(x - r_1)^3. \qquad (A.28)$$

On the basis of the arguments presented in Section 3, we make the guess for $f(x)$ as

$$f(x) \sim \frac{\alpha}{2r_1}(x^2 - r_1^2) + \frac{1}{\kappa^B}g(x). \qquad (A.29)$$

The integral equation (A.23) then takes the form

$$\frac{F}{p} = -\frac{Q^B}{\alpha p}\int_{r_1}^{\infty} dx \frac{d}{dx}\{exp - [p\alpha(x^2 - r_1^2)/2r_1]\}e^{-q^2 g(x)}r_1 W(x). \qquad (A.30)$$

The choice $g = w$ therefore makes the non-exact part of the integrand constant up to and including terms of order $O((x - r_1)^3)$, and the choice $\alpha = Q^B/F$ yields an approximate solution of the integral equation. In terms of the parameters introduced previously, the resulting solution for the front is of the form

$$\frac{4\kappa^B t}{r_1^2} = \frac{1}{\lambda_1}(\frac{x^2}{r_1^2} - 1) + 2(\frac{x}{r_1} - 1)^2 - \frac{2}{3}(\frac{x}{r_1} - 1)^3 + O((x/r_1 - 1)^4)). \qquad (A.31)$$

Writing $x = r_{ox}^B(t)$, this may be inverted to give

$$r_{ox}^B(t)^2 - r_1^2 = 4\kappa^B \lambda_1 t\{1 - \frac{\lambda_1 t}{2\tau} + \frac{\lambda_1^2 t^2}{2\tau^2}(1 + 2/\lambda)\} + O(t^4). \qquad (A.32)$$

This gives the solution for general values of the parameters, for small values of t. We note that the first 2 terms are consistent with (3.14), derived on the basis of the steady state approximation. The form of the expansion suggests that it gives reasonable answers for the front location provided the quantity $\frac{\lambda_1 t}{\tau}$ is small. In terms of the original parameters, the solution is valid for times t such that

$$t << \frac{D_{ox}^B}{\xi^B}(\frac{Q^B}{F})^2 \qquad (A.33)$$

A.2.2 Constant Flux: Large Times

The corresponding limit for large times may be deduced by considering the behaviour of the integral equation as p or q approach values where the integral is dominated by the contributions for large x. For the case of constant flux, the appropriate regime is given by taking p and q to approach zero. We proceed by considering the condition

$$\frac{d}{dq}\{p\bar{F}_{ox}(p)\} = 0, \tag{A.34}$$

as $q \longrightarrow 0$. By performing an expansion of the integral equation and changing variable to $y = qx$, the quantity $p\bar{F}_{ox}(p)$ can be written as

$$\frac{\kappa^B Q^B}{r_1}\int_{qr_1}^{\infty} ydy\epsilon xp\{-\kappa^B q^2 f(y/q)\}I_0(y)\{1 + \frac{q^2 r_1^2}{2} ln(\frac{qr_1}{2})\} \tag{A.35}$$

plus terms of higher order in q. Differentiating, and working to $O(qlnq)$, (A.34) is satisfied provided

$$\frac{\partial}{\partial q}[q^2 f(y/q)] \sim \frac{r_1^2}{\kappa^B} qln(qr_1/2), \quad q \longrightarrow 0. \tag{A.36}$$

This has the solution

$$f(x) \sim C\frac{x^2}{r_1^2} - \frac{r_1^2}{2\kappa^B} ln(x/r_1), \quad x \longrightarrow \infty. \tag{A.37}$$

The constant C may be determined by resubstitution in the undifferentiated form (A.35). The final result may be best expressed in forms analogous to (A.31) and (A.32). We have, respectively

$$\frac{4\kappa^B t}{r_1^2} \sim \frac{1}{\lambda_2}\frac{x^2}{r_1^2} - 2ln(\frac{x}{r_1}), \quad x \longrightarrow \infty \tag{A.38}$$

and inverse form

$$r_{ox}^B(t)^2 - r_1^2 \sim 4\kappa^B \lambda_2 t\{t + \lambda_1 \tau ln(t/\tau)\}, \quad t \longrightarrow \infty. \tag{A.39}$$

It may be verified that for small λ_1, this agrees with (3.14) to order λ_1^2 for large t.

A.2.3 Full Coupled Problem: Small Times; Effect of Canister

The initial behaviour of the front may be obtained, as before, by considering the behaviour of the integral equation, now (A.24), in the limit $p \longrightarrow \infty$. Now $G(p)$ satisfies

$$G(p) \sim \frac{G_0}{p}, p \longrightarrow \infty, \tag{A.40}$$

and this is exact if the production rate is constant. However, for any production rate expandable as a power series in t, an asymptotic expansion such as (A.40) will exist. By considering the first term only, with G_0 the oxidant production rate at time zero, the initial motion of the front may be obtained from (A.24) by letting $p \longrightarrow \infty$, and computing the derivative at $x = r_1$ of $f(x)$. If we write

$$r_{ox}^B(t)^2 - r_1^2 \sim 4\kappa^B \mu t, \tag{A.41}$$

then μ is determined by

$$\mu + \frac{\varepsilon^C}{\varepsilon^B}\mu^2 = \frac{r_1^2 G_0}{4\kappa^B Q^B} \tag{A.42}$$

If the oxidant production remains constant or subsequently decays, this equation may be considered as supplying an upper bound for the front velocity and location. The effect of the canister is to *slow* the front, and we note that if $\varepsilon^B = \varepsilon^C$, this effect may be regarded as taking the initial motion closer to that for the exact solution for a wire source (since $\mu + \mu^2$ is a better approximation to μe^μ than is μ.

A.2.4 Full Coupled Problem: Large Times with Low Production Decay

Another useful limiting case is obtained by considering the production decay times to be long compared with the times of interest in the front motion. If the oxidant production is set to a constant, the analogue of (A.38) may be obtained as

$$\frac{4\kappa^B t}{r_1^2} \sim \frac{1}{\Lambda_2}\frac{x^2}{r_1^2} - 2(1 - \varepsilon^C/\varepsilon^B) ln(x/r_1) + O(1) \tag{A.43}$$

where

$$\Lambda_2 exp \Lambda_2 = \frac{r_1^2 G_0}{4\kappa^B Q^B} \tag{A.44}$$

Here the effect of the canister is to modulate the size of the log term. If the two porosities are equal, the log term is zero, and the solution is very close to the exact solution for a wire with an equivalent production rate.

A.2.5 Summary

By use of an integral equation formalism, the motion of the front can be decoupled from the problem of computing the oxidant concentration behind the front. By use of the relations, the small-time behaviour can

be estimated for arbitrary flux or volume production rates, and large-time estimates for constant flux or volume production may be obtained easily. These estimates are valid for all values of the parameters of the problem, and are particularly useful for verifying computer algorithms.

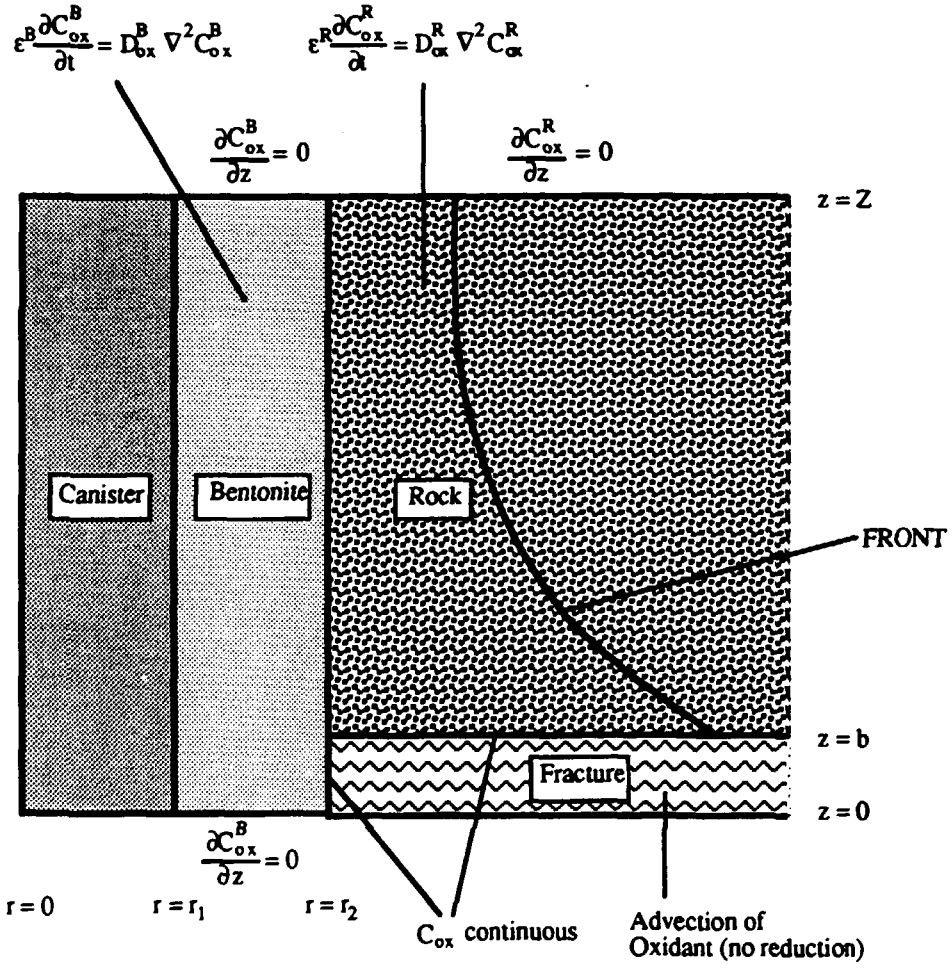

Figure 1: Microproblem for front calculations: advection in fracture

Symbol	Description	Units‡	Best Estimate	Range
A	Cylindrical surface area of canister	m^2	11.3	-
b	Half the fracture aperture	m	-	-
D_{ox}^{B}	Intrinsic diffusivity of oxidants in bentonite	$m^2.(ka)^{-1}$	1.3	$0.6 - 3.2$
D_{ox}^{R}	Intrinsic diffusivity of oxidants in rock matrix	$m^2.(ka)^{-1}$	1.6×10^{-3}	$(0.9 - 4) \times 10^{-3}$
$G_{ox}^{(t)}$	Oxidant production rate per m^3 of canister	$keq.m^{-3}.(ka)^{-1}$	0.32	$0.003 - 3.2$
L	Length of canister	m	4.5	
Q^B	Amount of oxidant which can be reduced per m^3 of bentonite	$keq.m^{-3}$	0.8	0.05 - 2
Q^C	Amount of oxidant which can be reduced per m^3 of canister	$keq.m^{-3}$	100	10-150
Q^R	Amount of oxidant which can be reduced per m^3 of rock matrix	$keq.m^{-3}$	5×10^{-2}	$0.01 - 3$
r_1	Radius of canister	m	0.4	-
r_2	Radius of bentonite/rock interface	m	0.74	-
r_3	Limit of matrix diffusion	m	-	-
V	Volume of canister	m^3	2.26	-
Z	Half the inter-fracture spacing	m	0.5	$0.05 - 5.0$
ε^B	Porosity of bentonite		0.35	$0.1 - 0.4$
ε^C	Porosity of degraded canister		10^{-2}	$10^{-3} - 10^{-1}$
ε^R	Porosity of rock matrix		10^{-3}	$10^{-4} - 10^{-2}$

‡1 ka = 1000 years $\sim 3.2 \times 10^{10} s$

Table 4: Initial parameter values for redox front calculations

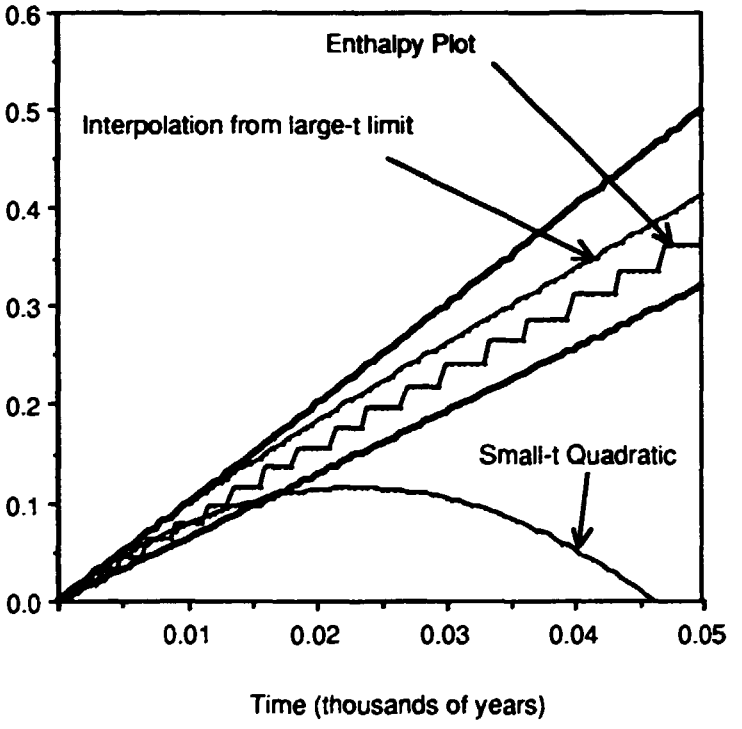

Figure 2: Cross-verification of Enthalpy Method and Analytical Results; $\lambda_1 = 0.69,\ \lambda_2 = 0.44,\ \tau = 16$years.

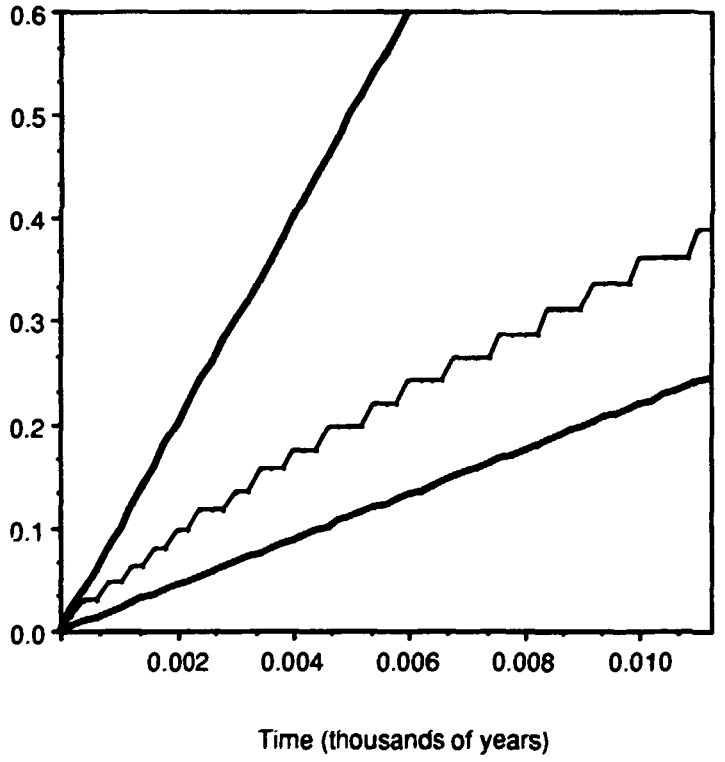

Figure 3: Cross-verification of Enthalpy Method and Analytical Results; $\lambda_1 = 6.9$, $\lambda_2 = 1.52$, $\tau = 1.6$years

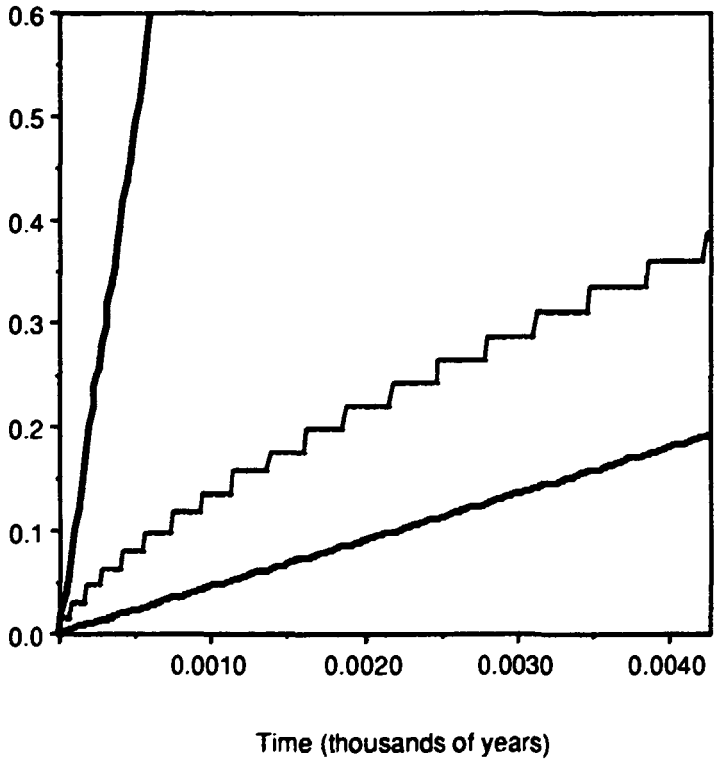

Figure 4: Cross-verification of Enthalpy Method and Analytical Results; $\lambda_1 = 69$, $\lambda_2 = 3.1$, $\tau = 0.16$ years.

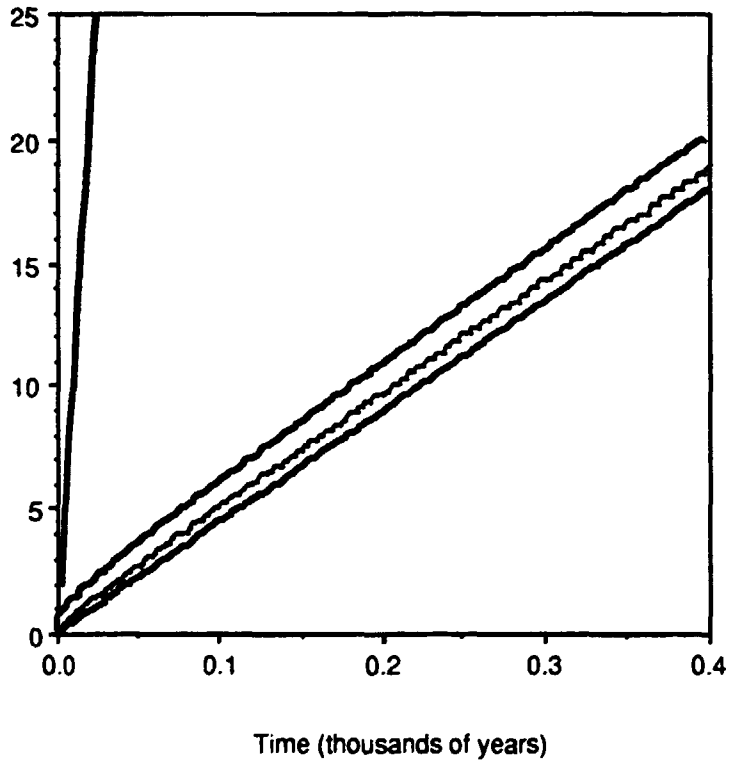

Figure 5: Cross-verification of Enthalpy Method and Analytical Results; $\lambda_1 = 69$, $\lambda_2 = 3.1$, $\tau = 0.16$ years.

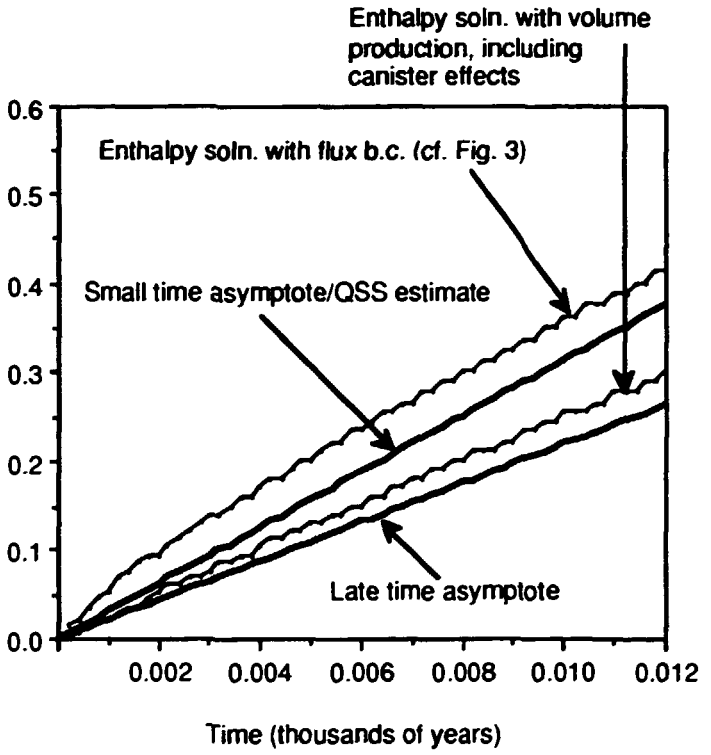

Figure 6: Cross-verification of Enthalpy Method and Analytical Results; Volume oxidant production with canister effects, $\varepsilon^C = \varepsilon^B$; $\lambda_1 = 6.9$, $\mu = 2.2$, $\lambda_2 = 1.52$.

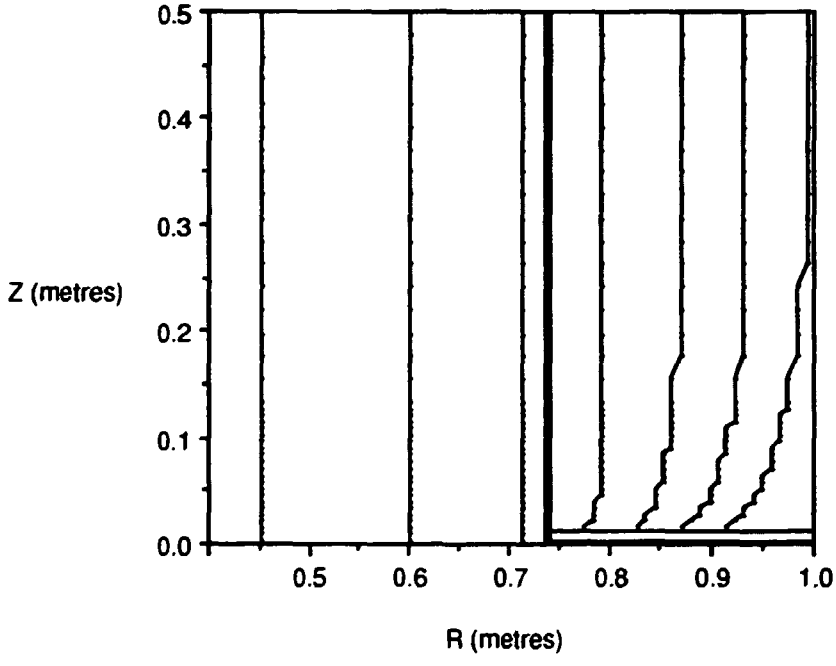

Figure 7: Example of 2D front motion; Front shown at equal time intervals; Rock and Bentonite parameters equal; original zero concentration boundary condition at fracture.

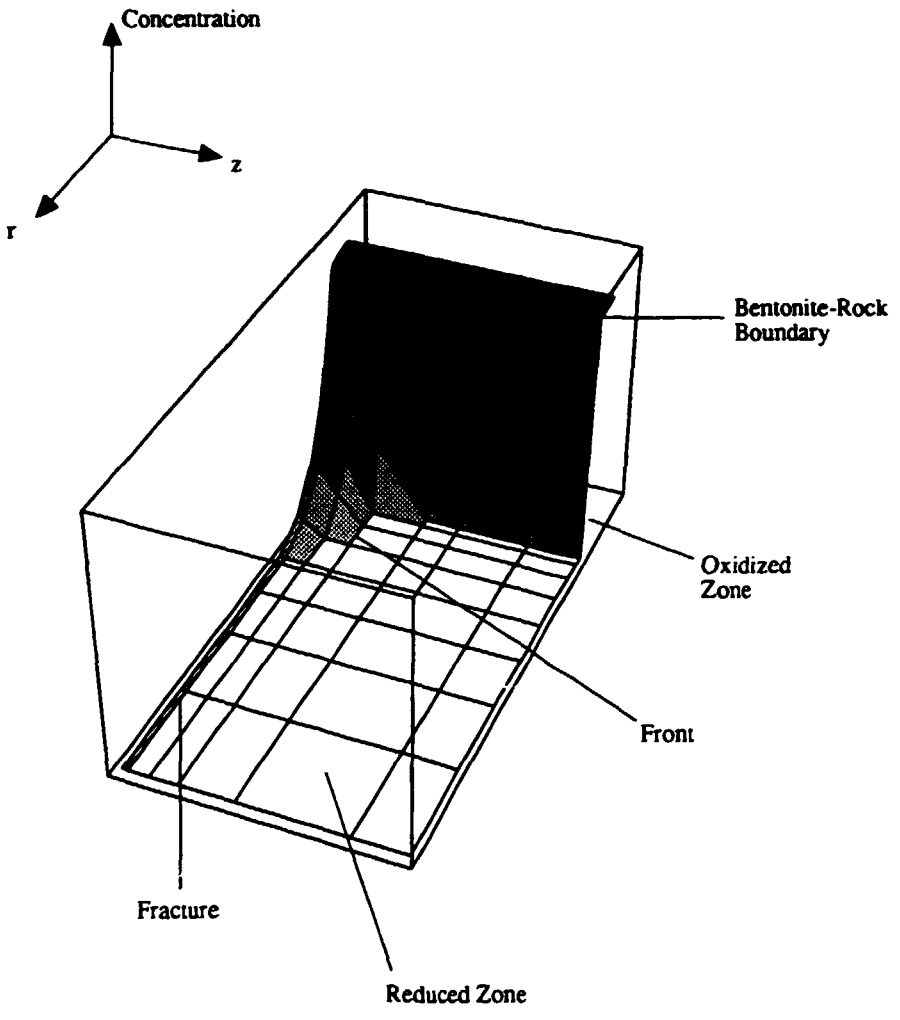

Figure 8: Typical concentration profile shortly after front escapes from bentonite; includes fracture transport effects.

References

[1] Hodgkinson, D.P., Robinson, P.C. & Pahwa, S.B. (1988), Preliminary Specification of a Source Term Model for the Swedish Spent Fuel Disposal Concept, INTERA-ECL Report I1794-1, Version 2, July 1988.

[2] SKBF/KBS (1983), Final Storage of Spent Nuclear Fuel - KBS-3, *i* General, *ii* Geology, *iii* Barriers, *iv* Safety, 1983.

[3] Shaw, W.T. (1989), Redox Front Motion in a System of Bentonite and Fractured Rock, SKI TR 89: 7, 1989.

[4] Shaw, W.T. (1992), The Oxidation State of the Near-field Environment in the CALIBRE Source Term Model: Further Remarks. SKI TR 91:20, 1992.

[5] Worgan, K.J. & Robinson, P.C. (1992), The CALIBRE Source-Term Code Technical Documentation for Project-90. SKI TR 91:18, 1992.

[6] Neretnieks, I. (1983), The Movement of a Redox Front Downstream from a Repository for Nuclear Waste. *Nuclear Technology* **62**, 110, 1983.

[7] Shaw, W., Smith, G., Worgan, K., Hodgkinson, D. and Andersson, K. (1992), Source Term Modelling Parameters for Project-90, SKI TR 91:27, 1992.

[8] Hill, J.M. (1984), *Math. Scientist* **9**, 15, 1984.

[9] Hill, J.M. & Dewynne, J.N. (1985), A note on Langford's Cylinder Functions $c_n(z, z_0)$ and $e_n(z, z_0)$, *Quarterly Journal of Applied Mathematics* **XLIII, 2**, 179, July 1985.

[10] Dewynne, J.N. & Hill, J.M. (1985), Bounds for Moving Boundary Problems with Two Chemical Reactions, *Nonlinear Analysis, Theory, Methods & Applications* **9, 11**, 1293, 1985.

[11] Carslaw, H.S. &Jaeger, J.C. (1959), *Conduction of Heat in Solids*, Clarendon Press, Oxford, 1959.

[12] Grinberg, G.A. & Chekmerava, O.M. (1971), *Sov. Phys. Tech. Phys.* **15**, 1579, 1971.

[13] Ockendon, J.R. (1974), Techniques of Analysis, in *Moving Boundary Problems in Heat Flow & Diffusion* ed. J.R. Ockendon & W.R. Hodgkins, Oxford, 1974.

[14] Crowley, A.B. & Ockendon, J.R., A Stefan Problem with a Non-monotone boundary. *J. Inst. Maths. Applics.* **20**, 269.

[15] Eyres, N.R., Hartree, D.R., Ingham, J., Jackson, R., Sargent, R.J. &Wagstaff, S.M. (1986), *Phil. Trans. R. Soc.* **A240**, 1, 1986.

[16] Atthey, D.R. 1974), *J. Inst. Math. Appl.* **13**, 353, 1974.

[17] Crank, J. (1984), *Free and Moving Boundary Value Problems*, Clarendon Press, Oxford, 1984.

[18] Abramowitz, M. & Stegun, I.A. (ed.) (1972), *Handbook of Mathematical Functions*. Dover, New York, 1972.

[19] Worgan, K. & Robinson, P. (1989), Preliminary Source Term Calculations for Project-90 using CALIBRE. INTERA-ECL Report I2211-3, Version 1, October 1989, Version 2 December 1989

[20] Christensen, H., Bjergbakke, E. (1982). Radiolysis of Groundwater from HLW stored in copper canisters, Studsvik Report Studsvik/NW-82/273, 1982.

[21] Christensen, H., Bjergbakke, E. (1982), Radiolysis of Groundwater from Spent Fuel, Studsvik Report Studsvik/NW-82/364, 1982.

[22] Christensen, H. & Bjergbakke, E. (1986), Application of Chemsimul for Groundwater Radiolysis, *Nucl. & Chem. Waste Mgment.* **6**, 265, 1986.

[23] Andersson, G., Neretnieks, I. & Rasmuson, A. (1982), SKBF-KBS Technical Report TR82-24, 1982.

[24] Christensen, H., private communication, 1989.

[25] Andersson, K., private communivation, August 1989.

SKi STATENS KÄRNKRAFTINSPEKTION
Swedish Nuclear Power Inspectorate

Postal address	Office	Telephone	Telex	Telefax
Box 27106 S-102 52 Stockholm	Sehlstedtsgatan 11	+46-8 665 44 00	11961 SWEATOM S	+46-8 661 90 86